
Persistence Fisher Kernel: A Riemannian Manifold Kernel for Persistence Diagrams

Tam Le

RIKEN Center for Advanced Intelligence Project, Japan
tam.le@riken.jp

Makoto Yamada

Kyoto University, Japan
RIKEN Center for Advanced Intelligence Project, Japan
makoto.yamada@riken.jp

Abstract

Algebraic topology methods have recently played an important role for statistical analysis with complicated geometric structured data such as shapes, linked twist maps, and material data. Among them, *persistent homology* is a well-known tool to extract robust topological features, and outputs as *persistence diagrams* (PDs). However, PDs are point multi-sets which can not be used in machine learning algorithms for vector data. To deal with it, an emerged approach is to use kernel methods, and an appropriate geometry for PDs is an important factor to measure the similarity of PDs. A popular geometry for PDs is the *Wasserstein metric*. However, Wasserstein distance is not *negative definite*. Thus, it is limited to build positive definite kernels upon the Wasserstein distance *without approximation*. In this work, we rely upon the alternative *Fisher information geometry* to propose a positive definite kernel for PDs *without approximation*, namely the Persistence Fisher (PF) kernel. Then, we analyze eigensystem of the integral operator induced by the proposed kernel for kernel machines. Based on that, we derive generalization error bounds via covering numbers and Rademacher averages for kernel machines with the PF kernel. Additionally, we show some nice properties such as stability and infinite divisibility for the proposed kernel. Furthermore, we also propose a linear time complexity over the number of points in PDs for an approximation of our proposed kernel with a bounded error. Throughout experiments with many different tasks on various benchmark datasets, we illustrate that the PF kernel compares favorably with other baseline kernels for PDs.

1 Introduction

Using algebraic topology methods for statistical data analysis has been recently received a lot of attention from machine learning community [Chazal et al., 2015, Kwitt et al., 2015, Bubenik, 2015, Kusano et al., 2016, Chen and Quadrianto, 2016, Carriere et al., 2017, Hofer et al., 2017, Adams et al., 2017, Kusano et al., 2018]. Algebraic topology methods can produce a robust descriptor which can give useful insight when one deals with complicated geometric structured data such as shapes, linked twist maps, and material data. More specifically, algebraic topology methods are applied in various research fields such as biology [Kasson et al., 2007, Xia and Wei, 2014, Cang et al., 2015], brain science [Singh et al., 2008, Lee et al., 2011, Petri et al., 2014], and information science [De Silva et al., 2007, Carlsson et al., 2008], to name a few.

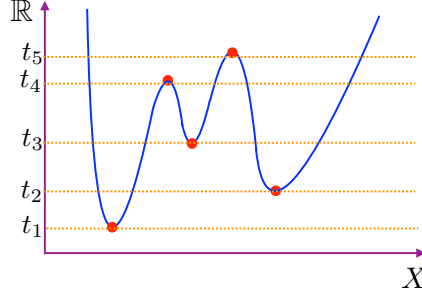


Figure 1: An illustration of a persistence diagram on a real-value function f . The orange horizontal lines are the boundaries of sublevel sets $f^{-1}((-\infty, t])$. For the 0-dimensional topological features (connected components), the topological events of births are happened at $t = t_1, t_2, t_3$ and their corresponding topological events of deaths are occurred at $t = +\infty, t_5, t_4$ respectively. Therefore, the persistent diagram of f is $\text{Dg}f = \{(t_1, +\infty), (t_2, t_5), (t_3, t_4)\}$.

In algebraic topology, *persistent homology* is an important method to extract robust topological information, it outputs point multisets, called *persistence diagrams* (PDs) [Edelsbrunner et al., 2000]. Since PDs can have different number of points, it is not straightforward to plug PDs into traditional statistical machine learning algorithms, which often assume a vector representation for data.

Related work. There are two main approaches in topological data analysis: (i) explicit vector representation for PDs such as computing and sampling functions built from PDs (i.e. persistence landscapes [Bubenik, 2015], tangent vectors from the mean of the square-root framework with principal geodesic analysis [Anirudh et al., 2016], or persistence images [Adams et al., 2017]), using points in PDs as roots of a complex polynomial for concatenated-coefficient vector representations [Di Fabio and Ferri, 2015], or using distance matrices of points in PDs for sorted-entry vector representations [Carriere et al., 2015], (ii) implicit representation via kernels such as the Persistence Scale Space (PSS) kernel, motivated by a heat diffusion problem with a Dirichlet boundary condition [Reininghaus et al., 2015], the Persistence Weighted Gaussian (PWG) kernel via kernel mean embedding [Kusano et al., 2016], or the Sliced Wasserstein (SW) kernel under Wasserstein geometry [Carriere et al., 2017]. In particular, geometry on PDs plays an important role. One of the most popular geometries for PDs is the Wasserstein metric [Villani, 2003, Peyre and Cuturi, 2017]. However, it is well-known that the Wasserstein distance is not *negative definite* [Reininghaus et al., 2015] (Appendix A). Consequently, we may not obtain positive definite kernels, built upon from the Wasserstein distance. Thus, it may be necessary to *approximate* the Wasserstein distance to achieve positive definiteness for kernels, relied on Wasserstein geometry. For example, [Carriere et al., 2017] used the SW distance—an *approximation* of Wasserstein distance—to construct the positive definite SW kernel.

Contributions. In this work, we focus on the implicit representation via kernels for PDs approach, and follow Anirudh et al. [2016] to explore an alternative Riemannian geometry, namely the Fisher information metric [Amari and Nagaoka, 2007, Lee, 2006] for PDs. Our contribution is two-fold: (i) we propose a positive definite kernel, namely the Persistence Fisher (PF) kernel for PDs. The proposed kernel well preserves the geometry of the Riemannian manifold since it is directly built upon the Fisher information metric for PDs *without approximation*. (ii) We analyze the eigensystem of the integral operator induced by the PF kernel for kernel machines. Based on that, we derive generalization error bounds via covering numbers and Rademacher averages for kernel machines with the PF kernel. Additionally, we provide some nice properties such as a bound for the proposed kernel induced squared distance with respect to the geodesic distance which can be interpreted as stability in a similar sense as the work of [Kwitt et al., 2015, Reininghaus et al., 2015] with Wasserstein geometry, and infinite divisibility for the proposed kernel. Furthermore, we describe a linear time complexity over the number of points in PDs for an approximation of the PF kernel with a bounded error via Fast Gauss Transform [Greengard and Strain, 1991, Morariu et al., 2009].

2 Background

Persistence diagrams. Persistence homology (PH) [Edelsbrunner and Harer, 2008] is a popular technique to extract robust topological features (i.e. connected components, rings, cavities) on real-value functions. Given $f : X \mapsto \mathbb{R}$, PH considers the family of *sublevel sets* of f (i.e.

$f^{-1}((-\infty, t]), t \in \mathbb{R}$) and records all *topological events* (i.e. births and deaths of topological features) in $f^{-1}((-\infty, t])$ when t goes from $-\infty$ to $+\infty$. PH outputs a 2-dimensional point multiset, called *persistence diagram* (PD), illustrated in Figure 3, where each 2-dimensional point represents a lifespan of a particular topological feature with its birth and death time as its coordinates.

Wasserstein geometry. Persistence diagram Dg can be considered as a discrete measure $\mu_{Dg} = \sum_{u \in Dg} \delta_u$ where δ_u is the Dirac unit mass on u . Therefore, the bottleneck metric (a.k.a. ∞ -Wasserstein metric) is a popular choice to measure distances on the set of PDs with bounded cardinalities. Given two PDs Dg_i and Dg_j , the bottleneck distance \mathcal{W}_∞ [Cohen-Steiner et al., 2007, Carriere et al., 2017, Adams et al., 2017] is defined as

$$\mathcal{W}_\infty(Dg_i, Dg_j) = \inf_{\gamma} \sup_{x \in Dg_i \cup \Delta} \|x - \gamma(x)\|_\infty,$$

where $\Delta := \{(a, a) \mid a \in \mathbb{R}\}$ is the diagonal set, and $\gamma : Dg_i \cup \Delta \rightarrow Dg_j \cup \Delta$ is bijective.

Fisher information geometry. Given a bandwidth $\sigma > 0$, for a set Θ , one can smooth and normalize μ_{Dg} as follows,

$$\rho_{Dg} := \left[\frac{1}{Z} \sum_{u \in Dg} N(x; u, \sigma I) \right]_{x \in \Theta}, \quad (1)$$

where $Z = \int_{\Theta} \sum_{u \in Dg} N(x; u, \sigma I) dx$, N is a Gaussian function and I is an identity matrix. Therefore, each PD can be regarded as a point in a probability simplex $\mathbb{P} := \{\rho \mid \int \rho(x) dx = 1, \rho(x) \geq 0\}^1$. In case, one chooses Θ as an entire Euclidean space, each PD turns into a probability distribution as in [Anirudh et al., 2016, Adams et al., 2017].

Fisher information metric (FIM)² is a well-known Riemannian geometry on the probability simplex \mathbb{P} , especially in information geometry [Amari and Nagaoka, 2007]. Given two points ρ_i and ρ_j in \mathbb{P} , the Fisher information metric is defined as

$$d_{\mathcal{P}}(\rho_i, \rho_j) = \arccos\left(\int \sqrt{\rho_i(x)\rho_j(x)} dx\right). \quad (2)$$

3 Persistence Fisher Kernel (PF Kernel)

In this section, we propose the Persistence Fisher (PK) kernel for persistence diagrams (PDs).

For the bottleneck distance, two PDs Dg_i and Dg_j may be two discrete measures with different masses. So, the transportation plan γ is bijective between $Dg_i \cup \Delta$ and $Dg_j \cup \Delta$ instead of between Dg_i and Dg_j . Carriere et al. [2017], for instance, used Wasserstein distance between Dg_i and Dg_j where its transportation plans operate between $Dg_i \cup Dg_{j\Delta}$ and $Dg_j \cup Dg_{i\Delta}$ (nonnegative, not necessarily normalized measures with same masses). Here, we denote $Dg_{i\Delta} := \{\Pi_\Delta(u) \mid u \in Dg_i\}$ where $\Pi_\Delta(u)$ is a projection of a point u on the diagonal set Δ . Following this line of work, we also consider a distance between two measures $Dg_i \cup Dg_{j\Delta}$ and $Dg_j \cup Dg_{i\Delta}$ as a distance between Dg_i and Dg_j for the Fisher information metric.

Definition 1. Let Dg_i, Dg_j be two finite and bounded persistence diagrams. The Fisher information metric between Dg_i and Dg_j is defined as follows,

$$d_{FIM}(Dg_i, Dg_j) := d_{\mathcal{P}}\left(\rho_{(Dg_i \cup Dg_{j\Delta})}, \rho_{(Dg_j \cup Dg_{i\Delta})}\right). \quad (3)$$

Lemma 3.1. Let \mathbb{D} be the set of bounded and finite persistent diagrams. Then, $(d_{FIM} - \tau)$ is negative definite on \mathbb{D} for all $\tau \geq \frac{\pi}{2}$.

Proof. Let consider the function $\tau - \arccos(\xi)$ where $\tau \geq \frac{\pi}{2}$ and $\xi \in [0, 1]$, then apply the Taylor series expansion for $\arccos(\xi)$ at 0, we have

$$\tau - \arccos(\xi) = \tau - \frac{\pi}{2} + \sum_{i=0}^{\infty} \frac{(2i)!}{2^{2i}(i!)^2(2i+1)} x^{2i+1}.$$

¹In case, Θ is an *infinite* set, then the corresponding probability simplex \mathbb{P} has *infinite* dimensions.

²FIM is also known as a particular pull-back metric on Riemannian manifold [Le and Cuturi, 2015b].

So, all coefficients of the Taylor series expansion are nonnegative. Following [Schoenberg, 1942] (Theorem 2, p. 102), for $\tau \geq \frac{\pi}{2}$ and $\xi \in [0, 1]$, $\tau - \arccos(\xi)$ is positive definite. Consequently, $\arccos(\xi) - \tau$ is negative definite. Furthermore, for any PDs Dg_i and Dg_j in \mathbb{D} , we have

$$0 \leq \int \sqrt{\bar{\rho}_i(x)\bar{\rho}_j(x)}dx \leq 1,$$

where we denote $\bar{\rho}_i = \rho_{(Dg_i \cup Dg_j \Delta)}$ and $\bar{\rho}_j = \rho_{(Dg_j \cup Dg_i \Delta)}$. The lower bound is due to nonnegativity of the probability simplex while the upper bound follows from the Cauchy-Schwarz inequality. Hence, $d_{\text{FIM}} - \tau$ is negative definite on \mathbb{D} for all $\tau \geq \frac{\pi}{2}$. ■

Based on Lemma 3.1, we propose a positive definite kernel for PDs under the Fisher information geometry by following [Berg et al., 1984] (Theorem 3.2.2, p.74), namely the Persistence Fisher kernel,

$$k_{\text{PF}}(Dg_i, Dg_j) := \exp(-td_{\text{FIM}}(Dg_i, Dg_j)), \quad (4)$$

where t is a positive scalar since we can rewrite the Persistence Fisher kernel as $k_{\text{PF}}(Dg_i, Dg_j) = \alpha \exp(-t(d_{\text{FIM}}(Dg_i, Dg_j) - \tau))$ where $\tau \geq \frac{\pi}{2}$ and $\alpha = \exp(-t\tau) > 0$.

To the best of our knowledge, the k_{PF} is the first kernel relying on the Fisher information geometry for measuring the similarity of PDs. Moreover, the k_{PF} is positive definite *without any approximation*.

Remark 1. Let $\mathbb{S}_+ := \{\nu \mid \int \nu^2(x)dx = 1, \nu(x) \geq 0\}$ be the positive orthant of the sphere, and define the Hellinger mapping $h(\cdot) := \sqrt{\cdot}$, where the square root is an element-wise function which transforms the probability simplex \mathbb{P} into \mathbb{S}_+ . The Fisher information metric between ρ_i and ρ_j in \mathbb{P} (Equation (2)) is equivalent to the geodesic distance between $h(\rho_i)$ and $h(\rho_j)$ in \mathbb{S}_+ . From [Levy and Loeve, 1965], the geodesic distance in \mathbb{S}_+ is a measure definite kernel distance. Following [Istas, 2012] (Proposition 2.8), the geodesic distance in \mathbb{S}_+ is negative definite. This result is also noted in [Feragen et al., 2015]. From [Berg et al., 1984] (Theorem 3.2.2, p.74), the Persistence Fisher kernel is positive definite. Therefore, our proof technique is not only independent and direct for the Fisher information metric on the probability simplex without relying on the geodesic distance on \mathbb{S}_+ , but also valid for the case of infinite dimensions due to [Schoenberg, 1942] (Theorem 2, p. 102).

Remark 2. A closely related kernel to the Persistence Fisher kernel is the diffusion kernel [Lafferty and Lebanon, 2005] (p. 140), based on the heat equation on the Riemannian manifold defined by the Fisher information metric to exploit the geometric structure of statistical manifolds. A generalized family of kernels for the diffusion kernel is exploited in [Jayasumana et al., 2015, Feragen et al., 2015]. To the best of our knowledge, the diffusion kernel has not been used for measuring the similarity of PDs. If one uses the Fisher information metric (Definition 1) for PDs, and then plug the distance into the diffusion kernel, one obtains a similar form to our proposed Persistence Fisher kernel. A slight difference is that the diffusion kernel relies on d_{FIM}^2 while the Persistence Fisher kernel is built upon d_{FIM} itself. However, the Persistence Fisher kernel is positive definite while it is unclear whether the diffusion kernel is positive definite³.

Computation. Given two finite PDs Dg_i and Dg_j with cardinalities bounded by N , in practice, we consider a finite set $\Theta := Dg_i \cup Dg_j \Delta \cup Dg_j \cup Dg_i \Delta$ without multiplicity in \mathbb{R}^2 for smoothed and normalized measures $\rho_{(\cdot)}$ (Equation 1)⁴. Then, let m be the cardinality of Θ , we have $m \leq 4N$. Consequently, the time complexity of $\rho_{(\cdot)}$ is $O(Nm)$. For acceleration, we propose to apply the Fast Gauss Transform [Greengard and Strain, 1991, Morariu et al., 2009] to approximate the sum of Gaussian functions in $\rho_{(\cdot)}$ with a bounded error. The time complexity of $\rho_{(\cdot)}$ is reduced from $O(Nm)$ to $O(N + m)$. Due to the low dimension of points in PDs (\mathbb{R}^2), this approximation by the Fast Gauss Transform is very efficient in practice. Additionally, $d_{\mathcal{P}}$ (Equation (2)) is evaluated between two points in the m -dimensional probability simplex \mathbb{P}_{m-1} where $\mathbb{P}_{m-1} := \{x \mid x \in \mathbb{R}_+^m, \|x\|_1 = 1\}$. So, the time complexity of the Persistence Fisher kernel k_{PF} between two smoothed and normalized measures is $O(m)$. Hence, the time complexity of k_{PF} between Dg_i and Dg_j is $O(N^2)$, or $O(N)$ for the acceleration version with Fast Gauss Transform. We summarize the computation of d_{FIM} in Algorithm

³Although the heat kernel is positive definite, the diffusion kernel on the probability simplex—the heat kernel on multinomial manifold—does not have an explicit form. In practice, the diffusion kernel equation [Lafferty and Lebanon, 2005] (p. 140) is only its first-order approximation.

⁴We leave the computation with an *infinite* set Θ for future work.

Table 1: A comparison for time complexities and metric preservation of kernels for PDs. Noted that the SW kernel is built upon the SW distance (an *approximation* of Wasserstein metric) while the PF kernel uses the Fisher information metric *without approximation*.

	k_{PSS}	k_{PWG}	k_{SW}	k_{PF}
Time complexity	$O(N^2)$	$O(N^2)$	$O(N^2 \log N)$	$O(N^2)$
Time complexity with approximation	$O(N)$	$O(N)$	$O(MN \log N)$	$O(N)$
Metric preservation			✓	✓

1, where the second and third steps can be approximated with a bounded error via Fast Gaussian Transform with a linear time complexity $O(N)$. Source code for Algorithm 1 can be obtained in <http://github.com/lttam/PersistenceFisher>. We recall that the time complexity of the Wasserstein distance between Dg_i and Dg_j is $O(N^3 \log N)$ [Pele and Werman, 2009] (§2.1). For the Sliced Wasserstein distance (an approximation of Wasserstein distance), the time complexity is $O(N^2 \log N)$ [Carriere et al., 2017], or $O(MN \log N)$ for its approximation with M projections [Carriere et al., 2017]. We also summary a comparison for the time complexity and metric preservation of k_{PF} and related kernels for PDs in Table 1.

Algorithm 1 Compute d_{FIM} for persistence diagrams

Input: Persistence diagrams Dg_i, Dg_j , and a bandwidth $\sigma > 0$ for smoothing

Output: d_{FIM}

- 1: Let $\Theta \leftarrow \text{Dg}_i \cup \text{Dg}_j \cup \text{Dg}_i \cup \text{Dg}_j$ (a set for smoothed and normalized measures)
 - 2: Compute $\bar{\rho}_i = \rho_{(\text{Dg}_i \cup \text{Dg}_j \cup \text{Dg}_i \cup \text{Dg}_j)} \leftarrow \left[\frac{1}{Z} \sum_{u \in \text{Dg}_i \cup \text{Dg}_j \cup \text{Dg}_i \cup \text{Dg}_j} \mathbb{N}(x; u, \sigma I) \right]_{x \in \Theta}$
where $Z \leftarrow \sum_{x \in \Theta} \sum_{u \in \text{Dg}_i \cup \text{Dg}_j \cup \text{Dg}_i \cup \text{Dg}_j} \mathbb{N}(x; u, \sigma I)$
 - 3: Compute $\bar{\rho}_j = \rho_{(\text{Dg}_j \cup \text{Dg}_i \cup \text{Dg}_j \cup \text{Dg}_i)}$ similarly as $\bar{\rho}_i$.
 - 4: Compute $d_{\text{FIM}} \leftarrow \arccos(\langle \sqrt{\bar{\rho}_i}, \sqrt{\bar{\rho}_j} \rangle)$ where $\langle \cdot, \cdot \rangle$ is a dot product and $\sqrt{\cdot}$ is element-wise.
-

4 Theoretical Analysis

In this section, we analyze for the Persistence Fisher kernel k_{PF} (in Equation (4)) where the Hellinger mapping h of a smoothed and normalized measure $\rho_{(\cdot)}$ is on the positive orthant of the d -dimension unit sphere \mathbb{S}_{d-1}^+ where $\mathbb{S}_{d-1}^+ := \{x \mid x \in \mathbb{R}_+^d, \|x\|_2 = 1\}$ ⁵. Let Dg_i, Dg_j be PDs in the set \mathbb{D} of bounded and finite PDs, and μ be the uniform probability distribution on \mathbb{S}_{d-1}^+ . We denote x_i and $x_j \in \mathbb{S}_{d-1}^+$ as corresponding mapped points through the Hellinger mapping h of smoothed and normalized measures $\rho_{(\text{Dg}_i \cup \text{Dg}_j \cup \text{Dg}_i \cup \text{Dg}_j)}$ and $\rho_{(\text{Dg}_j \cup \text{Dg}_i \cup \text{Dg}_j \cup \text{Dg}_i)}$ respectively. Then, we rewrite the Persistence Fisher kernel between x_i and x_j as follows,

$$k_{\text{PF}}(x_i, x_j) = \exp(-t \arccos(\langle x_i, x_j \rangle)). \quad (5)$$

Eigensystem. Let $T_{k_{\text{PF}}} : L_2(\mathbb{S}_{d-1}^+, \mu) \rightarrow L_2(\mathbb{S}_{d-1}^+, \mu)$ be the integral operator induced by the Persistence Fisher kernel k_{PF} , which is defined as

$$(T_{k_{\text{PF}}} f)(\cdot) := \int k_{\text{PF}}(x, \cdot) f(x) d\mu(x).$$

Following [Smola et al., 2001] (Lemma 4), we derive an eigensystem of the integral operator $T_{k_{\text{PF}}}$ as in Proposition 1.

Proposition 1. Let $\{a_i\}_{i \geq 0}$ be the coefficients of Legendre polynomial expansion of the Persistence Fisher kernel $k_{\text{PF}}(x, z)$ defined on $\mathbb{S}_{d-1}^+ \times \mathbb{S}_{d-1}^+$ as in Equation (5),

$$k_{\text{PF}}(x, z) = \sum_{i=0}^{\infty} a_i P_i^d(\langle x, z \rangle), \quad (6)$$

⁵It is corresponding to a finite set Θ .

where P_i^d is the associated Legendre polynomial of degree i . Let $|\mathbb{S}_{d-1}| := \frac{2\pi^{d/2}}{\Gamma(d/2)}$ denote the surface of \mathbb{S}_{d-1} where $\Gamma(\cdot)$ is the Gamma function, $N(d, i) := \frac{(d+2i-2)(d+i-3)!}{(d-2)!i!}$ denote the multiplicity of spherical harmonics of order i on \mathbb{S}_{d-1} , and $\{Y_{i,j}^d\}_{1 \leq j \leq N(d,i)}$ denote any fixed orthonormal basis for the subspace of all homogeneous harmonics of order i on \mathbb{S}_{d-1} . Then, the eigensystem $(\lambda_{i,j}, \phi_{i,j}^d)$ of the integral operator $T_{k_{\text{PF}}}$ induced by the Persistence Fisher kernel k_{PF} is

$$\phi_{i,j} = Y_{i,j}^d, \quad (7)$$

$$\lambda_{i,j} = \frac{a_i |\mathbb{S}_{d-1}|}{N(d, i)} \quad (8)$$

of multiplicity $N(d, i)$.

Proof. From the Addition Theorem [Muller, 2012] (Theorem 2, p. 18) and the Funk-Hecke formula [Muller, 2012] (§4, p. 29), we have $\sum_{j=1}^{N(d,i)} Y_{i,j}^d(x)Y_{i,j}^d(z) = \frac{N(d,i)}{|\mathbb{S}_{d-1}|} P_i^d(\langle x, z \rangle)$, then replace P_i^d into Equation (6), and note that $\int_{\mathbb{S}_{d-1}} Y_{i,j}^d(x)Y_{i',j'}^d(x)dx = \delta_{i,i'}\delta_{j,j'}$, we complete the proof. ■

Proposition 2. *All coefficients of Legendre polynomial expansion of the Persistence Fisher kernel are nonnegative.*

Proof. From Lemma 3.1, the k_{PF} is positive definite. Applying Schoenberg [1942] (Theorem 1, p. 101) for k_{PF} defined on $\mathbb{S}_{d-1}^+ \times \mathbb{S}_{d-1}^+$ as in Equation (5), we obtain the result. ■

The eigensystem of the integral operator $T_{k_{\text{PF}}}$ induced by the PF kernel plays an important role to derive generalization error bounds for kernel machines with the proposed PF kernel via covering numbers and Rademacher averages as in Proposition 3 and Proposition 4 respectively.

Covering numbers. Given a set of finite points $\mathcal{S} = \{x_i \mid x_i \in \mathbb{S}_{d-1}^+, d \geq 3\}$, the Persistence Fisher kernel hypothesis class with R -bounded weight vectors for \mathcal{S} is defined as follows

$$\mathcal{F}_R(\mathcal{S}) = \{\mathbf{f} \mid \mathbf{f}(x_i) = \langle w, \phi(x_i) \rangle_{\mathcal{H}}, \|w\|_{\mathcal{H}} \leq R\},$$

where $\langle \phi(x_i), \phi(x_j) \rangle_{\mathcal{H}} = k_{\text{PF}}(x_i, x_j)$. $\langle \cdot, \cdot \rangle_{\mathcal{H}}$ and $\|\cdot\|_{\mathcal{H}}$ are an inner product and a norm in the corresponding Hilbert space respectively. Following [Guo et al., 1999], we derive bounds on the generalization performance of the PF kernel on kernel machines via the covering numbers $\mathcal{N}(\cdot, \mathcal{F}_R(\mathcal{S}))$ [Shalev-Shwartz and Ben-David, 2014] (Definition 27.1, p. 337) as in Proposition 3.

Proposition 3. *Assume the number of non-zero coefficients $\{a_i\}$ in Equation (6) is finite, and r is the maximum index of the non-zero coefficients. Let $q := \arg \max_i \lambda_{i,\cdot}$, choose $\alpha \in \mathbb{N}$ such that $\alpha < \left(\frac{\lambda_{q,\cdot}}{\lambda_{i,\cdot}}\right)^{\frac{N(d,q)}{2}}$ with $i \neq q$, and define $\varepsilon := 6R\sqrt{N(d, r) \left(a_q \alpha^{-2/N(d,q)} + \sum_{i=0, i \neq q}^{\infty} a_i\right)}$. Then,*

$$\sup_{x_i \in \mathcal{S}} \mathcal{N}(\varepsilon, \mathcal{F}_R(\mathcal{S})) \leq \alpha.$$

Proof. From [Minh et al., 2006] (Lemma 3), we have $\|Y_{i,j}^d\|_{\infty} \leq \sqrt{\frac{N(d,i)}{|\mathbb{S}_{d-1}|}}$. It is easy to check that $\forall d \geq 3, i \geq j \geq 0$, we have $N(d, i) \geq N(d, j)$. Therefore, following Proposition 1, all eigenfunctions of k_{PF} satisfy that $\|Y_{i,j}^d\|_{\infty} \leq \sqrt{\frac{N(d,r)}{|\mathbb{S}_{d-1}|}}$. Additionally, the multiplicity of $\lambda_{i,\cdot}$ is $N(d, i)$, and $N(d, i)\lambda_{i,\cdot} = a_i |\mathbb{S}_{d-1}|$ (Equation (8)). Hence, from [Guo et al., 1999] (Theorem 1), we obtain the result. ■

Rademacher averages. We provide a different family of generalization error bounds via Rademacher averages [Bartlett et al., 2005]. By plugging the eigensystem of the PF kernel as in Proposition 1 into the localized averages of function classes based on the PF kernel with respect to the uniform probability distribution μ on \mathbb{S}_{d-1}^+ [Mendelson, 2003] (Theorem 2.1), we obtain a bound as in Proposition 4.

Proposition 4. Let $\{x_i\}_{1 \leq i \leq m}$ be independent, distributed according to the uniform probability distribution μ on \mathbb{S}_{d-1}^+ , denote $\{\sigma_i\}_{1 \leq i \leq m}$ for independent Rademacher random variables, $\mathcal{H}_{k_{PF}}$ for the unit ball of the reproducing kernel Hilbert space corresponding with the Riemannian manifold kernel k_{PF} , and let $q := \arg \max_i \lambda_{i,\cdot}$. If $\lambda_{q,\cdot} \geq 1/m$, for $\tau \geq 1/(m |\mathbb{S}_{d-1}|)$,

let $\Psi(\tau) := \sqrt{|\mathbb{S}_{d-1}| \left(\sum_{a_i < \tau N(d,i)} a_i + \tau \sum_{a_i \geq \tau N(d,i)} N(d,i) \right)}$, then there are absolute constants C_ℓ and C_u which satisfy

$$C_\ell \Psi(\tau) \leq \mathbb{E} \sup_{\substack{\mathbf{f} \in \mathcal{H}_{k_{PF}} \\ \frac{\mathbb{E} \mu \mathbf{f}^2}{|\mathbb{S}_{d-1}|} \leq \tau}} \left| \sum_{i=1}^m \sigma_i \mathbf{f}(x_i) \right| \leq C_u \Psi(\tau), \quad (9)$$

where \mathbb{E} is an expectation.

From Proposition 3 and Proposition 4, a decay rate of the eigenvalues of the integral operator $T_{k_{PF}}$ is relative with the capacity of the kernel learning machines. When the decay rate of the eigenvalues is large, the capacity of kernel machines is reduced. So, if the training error of kernel machines is small, then it can lead to better bounds on generalization error. The resulting bounds for both the covering number (Proposition 3) and the Rademacher averages (Proposition 4) are essentially the same as the standard ones for a Gaussian kernel on a Euclidean space.

Bounding for k_{PF} induced squared distance with respect to d_{FIM} . The squared distance induced by the PF kernel, denoted as $d_{k_{PF}}^2$, can be computed by the Hilbert norm of the difference between two corresponding mappings. Given two persistent diagram Dg_i and Dg_j , we have

$$d_{k_{PF}}^2(Dg_i, Dg_j) := k_{PF}(Dg_i, Dg_i) + k_{PF}(Dg_j, Dg_j) - 2k_{PF}(Dg_i, Dg_j).$$

We recall that k_{PF} is based on the Fisher information geometry. So, it is of interest to bound the PF kernel induced squared distance $d_{k_{PF}}^2$ with respect to the corresponding Fisher information metric d_{FIM} between PDs as in Lemma 4.1.

Lemma 4.1. Let \mathbb{D} be the set of bounded and finite persistent diagrams. Then, $\forall Dg_i, Dg_j \in X$,

$$d_{k_{PF}}^2(Dg_i, Dg_j) \leq 2td_{FIM}(Dg_i, Dg_j),$$

where t is a parameter of k_{PF} .

Proof. We have $d_{k_{PF}}^2(Dg_i, Dg_j) = 2(1 - k_{PF}(Dg_i, Dg_j)) = 2(1 - \exp(-td_{FIM}(Dg_i, Dg_j))) \leq 2td_{FIM}(Dg_i, Dg_j)$, since $1 - \exp(-a) \leq a, \forall a \geq 0$. ■

From Lemma 4.1, it implies that the Persistence Fisher kernel is stable on Riemannian geometry in a similar sense as the work of Kwitt et al. [2015], and Reininghaus et al. [2015] on Wasserstein geometry.

Infinite divisibility for the Persistence Fisher kernel.

Lemma 4.2. The Persistence Fisher kernel k_{PF} is infinitely divisible.

Proof. For $m \in \mathbb{N}^*$, let $k_{PF_m} := \exp(-\frac{t}{m}d_{FIM})$, so $(k_{PF_m})^m = k_{PF}$ and note that k_{PF_m} is positive definite. Hence, following Berg et al. [1984] (§3, Definition 2.6, p. 76), we have the result. ■

As for infinitely divisible kernels, the Gram matrix of the PF kernel does not need to be recomputed for each choice of t (Equation (4)), since it suffices to compute the Fisher information metric between PDs in training set only once. This property is shared with the Sliced Wasserstein kernel [Carriere et al., 2017]. However, neither Persistence Scale Space kernel [Reininghaus et al., 2015] nor Persistence Weighted Gaussian kernel [Kusano et al., 2016] has this property.

Table 2: Results on SVM classification. The averaged accuracy (%) and standard deviation are shown.

	MPEG7	Orbit
k_{PSS}	73.33 \pm 4.17	72.38 \pm 2.41
k_{PWG}	74.83 \pm 4.36	76.63 \pm 0.66
k_{SW}	76.83 \pm 3.75	83.60 \pm 0.87
Prob+ k_G	55.83 \pm 5.45	72.89 \pm 0.62
Tang+ k_G	66.17 \pm 4.01	77.32 \pm 0.72
k_{PF}	80.00 \pm 4.08	85.87 \pm 0.77

5 Experimental Results

We evaluated the Persistence Fisher kernel with support vector machines (SVM) on many benchmark datasets. We consider five baselines as follows: (i) the Persistence Scale Space kernel (k_{PSS}), (ii) the Persistence Weighted Gaussian kernel (k_{PWG}), (iii) the Sliced Wasserstein kernel (k_{SW}), (iv) the smoothed and normalized measures in the probability simplex with the Gaussian kernel (Prob + k_G), and (v) the tangent vector representation [Anirudh et al., 2016] with the Gaussian kernel (Tang + k_G). Practically, Euclidean metric is not a suitable geometry for the probability simplex [Le and Cuturi, 2015a,b]. So, the (Prob + k_G) approach may not work well for PDs. For hyper-parameters, we typically choose them through cross validation. For baseline kernels, we follow their corresponding authors to form sets of hyper-parameter candidates, and the bandwidth of the Gaussian kernel in (Prob + k_G) and (Tang + k_G) is chosen from $10^{\{-3:1:3\}}$. For the Persistence Fisher kernel, there are 2 hyper-parameters: t (Equation (4)) and σ for smoothing measures (Equation (1)). We choose $1/t$ from $\{q_1, q_2, q_5, q_{10}, q_{20}, q_{50}\}$ where q_s is the $s\%$ quantile of a subset of Fisher information metric between PDs, observed on the training set, and σ from $\{10^{-3:1:3}\}$. For SVM, we use Libsvm (one-vs-one) [Chang and Lin, 2011] for multi-class classification, and choose a regularization parameter of SVM from $\{10^{-2:1:2}\}$. For PDs, we used the DIPHA toolbox⁶.

5.1 Orbit Recognition

It is a synthesized dataset proposed by [Adams et al., 2017] (§6.4.1) for *linked twist map* which is a discrete dynamical system modeling flow. The linked twist map is used to model flows in DNA microarrays [Hertzsch et al., 2007]. Given a parameter $r > 0$, and initial positions $(s_0, t_0) \in [0, 1]^2$, its orbit is described as $s_{i+1} = s_i + rt_i(1 - t_i) \bmod 1$, and $t_{i+1} = t_i + rs_{i+1}(1 - s_{i+1}) \bmod 1$. Adams et al.

[2017] proposed 5 classes, corresponding to 5 different parameters $r = 2.5, 3.5, 4, 4.1, 4.3$. For each parameter r , we generated 1000 orbits where each orbit has 1000 points with random initial positions. We randomly split 70%/30% for training and test, and repeated 100 times. We extract only 1-dimensional topological features with Vietoris-Rips complex filtration [Edelsbrunner and Harer, 2008] for PDs. The accuracy results on SVM are summarized in the third column of Table 2. The PF kernel outperforms all other baselines. The (Prob + k_G) does not performance well as expected. Moreover, the k_{PF} and k_{SW} which enjoy the Fisher information geometry and Wasserstein geometry for PDs respectively, clearly outperform other approaches. As in the second column of Table 3, the computational time of k_{PF} is faster than k_{PSS} , but slower than k_{SW} and k_{PWG} for PDs.

Table 3: Computational time (seconds) with approximation. For each dataset, the first number in the parenthesis is the number of PDs while the second one is the maximum number of points in PDs.

	Orbit (5K/300)	MPEG7 (200/80)	Granular (35/20.4K)	SiO ₂ (80/30K)
k_{SW}	6473	1.55	8.30	249
k_{PWG}	8756	5.23	17.44	288
k_{PSS}	11024	7.51	38.14	515
k_{PF}	9891	6.63	22.70	318

5.2 Object Shape Classification

We consider a 10-class subset⁷ of MPEG7 object shape dataset [Latecki et al., 2000]. Each class has 20 samples. We resize each image such that its length is shorter or equal 256, and extract a boundary for object shapes before computing PDs. For simplicity, we only consider 1-dimensional topological

⁶<https://github.com/DIPHA/dipha>

⁷The 10-classes are: apple, bell, bottle, car, classic, cup, device0, face, Heart and key.

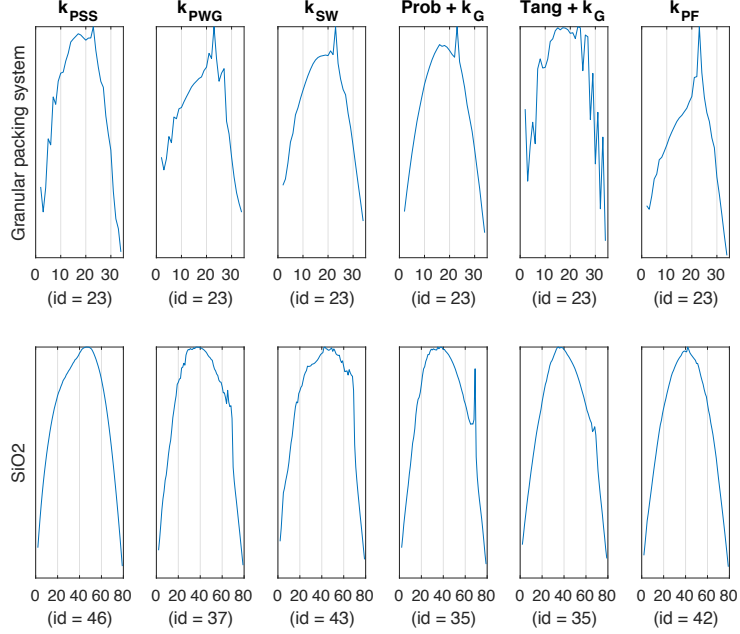


Figure 2: The kernel Fisher discriminant ratio (KFDR) graphs.

features with the traditional Vietoris-Rips complex filtration [Edelsbrunner and Harer, 2008] for PDs⁸. We also randomly split 70%/30% for training and test, and repeated 100 times. The accuracy results on SVM are summarized in the second column of Table 2. The Persistence Fisher kernel compares favorably with other baseline kernels for PDs. All approaches based on the implicit representation via kernels for PDs outperform ones based on the explicit vector representation with Gaussian kernel by a large margin. Additionally, the k_{PF} and k_{SW} also compares favorably with other approaches. As in the third column of Table 3, the computational time of k_{PF} is comparative with k_{PWG} and k_{PSS} , but slower than the k_{SW} .

5.3 Change Point Detection for Material Data Analysis

We evaluated the proposed kernel for the change point detection problem for material data analysis on granular packing system [Francois et al., 2013] and SiO_2 [Nakamura et al., 2015] datasets. We use the kernel Fisher discriminant ratio [Harchaoui et al., 2009] (KFDR) as a statistical quantity and set 10^{-3} for the regularization of KFDR as in [Kusano et al., 2018]. We use the ball model filtration to extract the 2-dimensional topological features of PDs for granular packing system dataset, and 1-dimensional topological features of PDs for SiO_2 dataset. We illustrate the KFDR graphs for the granular packing system and SiO_2 datasets in Figure 2. For granular tracking system dataset, all methods obtain the change point as the 23rd index. They supports the observation result in [Anonymous, 1972] (corresponding $\text{id} = 23$). For the SiO_2 datasets, all methods obtain the results within the supported range ($35 \leq \text{id} \leq 50$) from the traditional physical approach [Elliott, 1983]. The k_{PF} compares favorably with other baseline approaches as in Figure 2. As in the fourth and fifth columns of Table 3, k_{PF} is faster than k_{PSS} , but slower than k_{SW} and k_{PWG} .

6 Conclusions

In this work, we propose the positive definite Persistence Fisher (PF) kernel for persistence diagrams (PDs). The PF kernel is relied on the Fisher information geometry *without approximation* for PDs. Moreover, the proposed kernel has many nice properties from both theoretical and practical aspects such as stability, infinite divisibility, linear time complexity over the number of points in PDs, and improving performances of other baseline kernels for PDs as well as implicit vector representation with Gaussian kernel for PDs in many different tasks on various benchmark datasets.

⁸A more advanced filtration for this task was proposed in [Turner et al., 2014].

Acknowledgments

We thank Ha Quang Minh, and anonymous reviewers for their comments. TL acknowledges the support of JSPS KAKENHI Grant number 17K12745. MY was supported by the JST PRESTO program JPMJPR165A.

A Some Traditional Filtrations for Persistence Diagrams

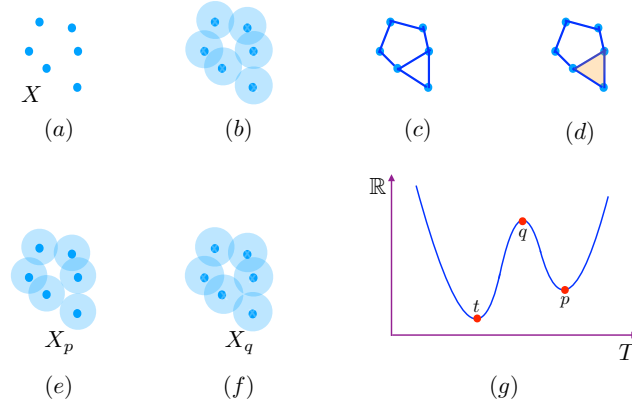


Figure 3: An illustration for persistence diagrams with some popular filtrations. (a) A set of points as an input. (b) A ball model filtration. (c) Cech complex filtration. (d) Vietoris-Rips complex filtration (it has only 1 ring since it contains a 2-simplex, illustrated as the orange triangle). (e) An illustration of a birth of a ring in the ball model filtration. (f) An illustration of a death for a ring in the ball model filtration. (g) A sub-level set filtration (a connected component has a birth at \mathfrak{F}_p , and a death at \mathfrak{F}_q). In this illustration, both the ball model filtration and Cech complex filtration have 2 rings, but there is only 1 ring for Vietoris-Rips complex filtration due to the 2-simplex. For sub-level set filtration, there are 2 connected components (p, q) and (t, ∞) . Hence, the persistence diagram of 0-dimensional topological feature is that $\text{Dg} = \{(p, q); (t, \infty)\}$.

We provide some traditional filtrations to illustrate persistence diagrams as follows,

Ball model filtration. Let $X = \{x_1, x_2, \dots, x_m\}$ be a finite set in a metric space as in Figure 3 (a), and $B(x, a)$ be a ball with a center x and a radius a . We denote $X_a := \cup_{x_i \in X} B(x_i, a)$ for $a \geq 0$. For $a < 0$, we define $X_a := \emptyset$. Therefore, $\{X_a \mid a \in \mathbb{R}\}$ can be used as a filtration, illustrated in Figure 3 (b). For example, Figure 3 (e) shows a birth for a ring at X_p while Figure 3 (f) illustrates that the ring is death at X_q . Therefore, a point (p, q) is in the persistence diagram of 1-dimensional topological feature for the set X .

Cech complex filtration. Given a set $X = \{x_1, x_2, \dots, x_m\}$ in a metric space (T, d_T) . For $a \geq 0$, we form a t -simplex from a $(t + 1)$ -point subset X_{t+1} of X if there exist $x' \in M$, such that $d_T(x, x') \leq a, \forall x \in X_{t+1}$. The set of all these simplices is called the Cech complex of X with parameter $a \geq 0$, denoted as $\mathfrak{C}(X, a)$. For $a < 0$, we definite $\mathfrak{C}(X, a) := \emptyset$. Therefore, $\{\mathfrak{C}(X, a) \mid a \in \mathbb{R}\}$ can be considered as a filtration and illustrated in Figure 3 (c). When $T \subset \mathbb{R}^q$, the topology of $\mathfrak{C}(X, a)$ is homotopy equivalent to X_a [Hatcher, 2002] (p. 257). Consequently, the persistence diagrams with Cech complex filtration equals to the persistence diagrams with ball model filtration.

Vietoris-Rips complex (a.k.a. Rips complex) filtration. Given a set $X = \{x_1, x_2, \dots, x_m\}$ in a metric space (T, d_T) . For $a \geq 0$, we form a t -simplex from a $(t + 1)$ -point subset X_{t+1} of X which satisfies $d_T(x, z) \leq 2a, \forall x, z \in X_{t+1}$. The set of all these simplices is called Vietoris-Rips complex of X with parameter $a \geq 0$, denoted as $\mathfrak{R}(X, a)$. For $a < 0$, we define $\mathfrak{R}(X, a) = \emptyset$. Therefore, $\{\mathfrak{R}(X, a) \mid a \in \mathbb{R}\}$ can be used as a filtration as illustrated in Figure 3 (d).

Sub-level set filtration. Let T be a topological space, given a function $f : T \rightarrow \mathbb{R}$ as an input, and defined a sub-level set $\mathfrak{F}_a := f^{-1}((-\infty, a])$. Thus, $\{\mathfrak{F}_a \mid a \in \mathbb{R}\}$ can be regarded as a filtration as in Figure 3 (g). For example, it is easy to see that a connected component has a birth at \mathfrak{F}_p and it is death at \mathfrak{F}_q as in Figure 3 (g). Thus, a point (p, q) is in persistence diagrams of 0-dimensional topological feature for the given function f . In Figure 3 (g), persistence diagram of 0-dimensional topological feature for f is $\text{Dg} = \{(p, q); (t, \infty)\}$.

B Kernels

We review some important definitions and theorems about kernels.

Positive definite kernels. A function $k : X \times X \rightarrow \mathbb{R}$ is called a positive definite kernel if $\forall n \in \mathbb{N}^*, \forall x_1, x_2, \dots, x_n \in X, \sum_{i,j} c_i c_j k(x_i, x_j) \geq 0, \forall c_i \in \mathbb{R}$.

Negative definite kernels. A function $k : X \times X \rightarrow \mathbb{R}$ is called a negative definite kernel if $\forall n \in \mathbb{N}^*, \forall x_1, x_2, \dots, x_n \in X, \sum_{i,j} c_i c_j k(x_i, x_j) \leq 0, \forall c_i \in \mathbb{R}$ such that $\sum_i c_i = 0$.

Berg-Christensen-Ressel Theorem. In [Berg et al., 1984] (Theorem 3.2.2, p.74), if κ is a *negative definite* kernel, then $k_t(x, z) := \exp(-t\kappa(x, z))$ is a positive definite kernel for all $t > 0$. For example, Gaussian kernel $k_t(x, z) = \exp\left(-t\|x - z\|_2^2\right)$ is positive definite since it is easy to check that squared Euclidean distance is indeed a negative definite kernel⁹.

Schoenberg Theorem. In [Schoenberg, 1942] (Theorem 2, p. 102), a function $f(\langle \cdot, \cdot \rangle)$ defined on the unit sphere in a Hilbert space is positive definite if and only if its Taylor series expansion has only nonnegative coefficients,

$$f(\xi) = \sum_{i=0}^{\infty} a_i \xi^i, \quad \text{with } a_i \geq 0. \quad (10)$$

C Related Kernels for Persistence Diagrams

Persistence Scale Space kernel (k_{PSS}). Reininghaus et al. [2015] proposed the Persistence Scale Space (PSS) kernel, motivated by a heat diffusion problem with a Dirichlet boundary condition. The PSS kernel between two PDs Dg_i and Dg_j is defined as $k_{\text{PSS}}(\text{Dg}_i, \text{Dg}_j) := \frac{1}{8\pi\sigma} \sum_{\substack{p_i \in \text{Dg}_i \\ p_j \in \text{Dg}_j}} \exp\left(-\frac{\|p_i - p_j\|_2^2}{8\sigma}\right) - \exp\left(-\frac{\|p_i - \bar{p}_j\|_2^2}{8\sigma}\right)$, where σ is a scale parameter and if $p = (a, b)$, then $\bar{p} = (b, a)$, mirrored at the diagonal Δ . The time complexity is $O(N^2)$ where N is the bounded cardinality of PDs. By using the Fast Gauss Transform [Greengard and Strain, 1991] for approximation with bounded error, the time complexity can be reduced to $O(N)$.

Persistence Weighted Gaussian kernel (k_{PWG}). Kusano et al. [2016] proposed the Persistence Weighted Gaussian (PWG) kernel by using kernel embedding into the reproducing kernel Hilbert space. Let k_{G_σ} be the Gaussian kernel with a positive parameter σ , and associated reproducing kernel Hilbert space \mathcal{H}_σ . Let $\mu_i := \sum_{p \in \text{Dg}_i} \arctan(C \text{pers}(p)^q) k_{G_\sigma}(\cdot, p) \in \mathcal{H}_\sigma$, where C, q are positive parameter, and for $p = (a, b)$, a persistence of p is that $\text{pers}(p) := b - a$. Let μ_j be defined similarly for Dg_j . Given a parameter $\tau > 0$, the persistence weighted Gaussian kernel is defined as $k_{\text{PWG}}(\text{Dg}_i, \text{Dg}_j) := \exp\left(-\frac{\|\mu_i - \mu_j\|_{\mathcal{H}_\sigma}^2}{2\tau^2}\right)$. The time complexity is $O(N^2)$. Furthermore, Kusano et al. [2016] also proposed to use the random Fourier features [Rahimi and Recht, 2008] for computing the Gram matrix of m persistent diagrams with $O(mNu + m^2u)$ complexity, where u is the number of random variables using for random Fourier features. Thus, the time complexity can be reduced to be linear in N .

⁹ $\forall n \in \mathbb{N}^*, \forall x_1, x_2, \dots, x_n \in X$, and $\forall c_i \in \mathbb{R}$ such that $\sum_i c_i = 0$, we have $\sum_{i,j} c_i c_j \|x_i - x_j\|_2^2 = \sum_i c_i x_i^2 \sum_j c_j + \sum_i c_i \sum_j c_j x_j^2 - 2 \sum_{i,j} c_i c_j x_i x_j = -2 (\sum_i c_i x_i)^2 \leq 0$.

Table 4: Averaged accuracy results (%) on SVM classification. The result of MTF with SVM is cited from [Cang et al., 2015].

	MTF	k_{PSS}	k_{PWG}	k_{SW}	Prob+ k_G	k_{PF}
Accuracy (%)	84.50	83.33	88.89	88.89	83.95	97.53

Sliced Wasserstein kernel (k_{SW}). Carriere et al. [2017] proposed the Sliced Wasserstein (SW) kernel, motivated from Wasserstein geometry for PDs. However, it is well-known that the Wasserstein distance is not negative definite. Therefore, it may be necessary to *approximate* the Wasserstein distance to design positive definite kernels on Wasserstein geometry for PDs. Indeed, Carriere et al. [2017] use the SW distance, which is an approximation of Wasserstein distance, for proposing the positive definite SW kernel, defined as $k_{\text{SW}}(\text{Dg}_i, \text{Dg}_j) := \exp\left(-\frac{d_{\text{SW}}(\text{Dg}_i, \text{Dg}_j)}{2\sigma^2}\right)$. The time complexity for the SW distance $d_{\text{SW}}(\text{Dg}_i, \text{Dg}_j)$ is $O(N^2 \log N)$, and for its M -projection approximation, it is $O(MN \log N)$.

Metric preservation. For those kernel methods for PDs, only the SW kernel preserves the metric between PDs, that is the Wasserstein geometry. Furthermore, Carriere et al. [2017] argued that this property should lead to improve the classification power. In this work, we explore an alternative Riemannian manifold geometry for PDs, namely the Fisher information metric which is also known as a particular pull-back metric on Riemannian manifold [Le and Cuturi, 2015b]. Moreover, the proposed positive definite Persistence Fisher kernel is directly built upon the Fisher information metric for PDs *without approximation* while it may be necessary to approximate the Wasserstein distance for designing positive definite kernels on Wasserstein geometry for PDs. Additionally, the time complexity of the Persistence Fisher kernel is also better than the Sliced Wasserstein kernel in term of computation.

D More Experiments on Hemoglobin Classification

We evaluated the Persistence Fisher kernel on Hemoglobin classification for the *taunt* and *relaxed* forms [Cang et al., 2015]. For each form, there are 9 data points, collected by the X-ray crystallography. As in [Kusano et al., 2018], we selected 1 data point from each class for test and used the rest for training. There are totally 81 runs. We also compared with the molecular topological fingerprint (MTF) for SVM [Cang et al., 2015]. We summarize averaged accuracy results on SVM in Table 4. The Persistence Fisher kernel again outperforms other baseline kernels, and also SVM with MTF.

References

- Henry Adams, Tegan Emerson, Michael Kirby, Rachel Neville, Chris Peterson, Patrick Shipman, Sofya Chepushtanova, Eric Hanson, Francis Motta, and Lori Ziegelmeier. Persistence images: A stable vector representation of persistent homology. *The Journal of Machine Learning Research*, 18(1):218–252, 2017.
- Shun-ichi Amari and Hiroshi Nagaoka. *Methods of information geometry*, volume 191. American Mathematical Soc., 2007.
- Rushil Anirudh, Vinay Venkataraman, Karthikeyan Natesan Ramamurthy, and Pavan Turaga. A riemannian framework for statistical analysis of topological persistence diagrams. In *Proceedings of the IEEE Conference on Computer Vision and Pattern Recognition Workshops*, pages 68–76, 2016.
- Anonymous. What is random packing? *Nature*, 239:488–489, 1972.
- Peter L Bartlett, Olivier Bousquet, Shahar Mendelson, et al. Local rademacher complexities. *The Annals of Statistics*, 33(4):1497–1537, 2005.
- Christian Berg, Jens Peter Reus Christensen, and Paul Ressel. *Harmonic analysis on semigroups*. Springer-Verlag, 1984.

- Peter Bubenik. Statistical topological data analysis using persistence landscapes. *The Journal of Machine Learning Research*, 16(1):77–102, 2015.
- Zixuan Cang, Lin Mu, Kedi Wu, Kristopher Opron, Keli Xia, and Guo-Wei Wei. A topological approach for protein classification. *Molecular Based Mathematical Biology*, 3(1), 2015.
- Gunnar Carlsson, Tigran Ishkhanov, Vin De Silva, and Afra Zomorodian. On the local behavior of spaces of natural images. *International journal of computer vision*, 76(1):1–12, 2008.
- Mathieu Carriere, Steve Y Oudot, and Maks Ovsjanikov. Stable topological signatures for points on 3d shapes. In *Computer Graphics Forum*, volume 34, pages 1–12. Wiley Online Library, 2015.
- Mathieu Carriere, Marco Cuturi, and Steve Oudot. Sliced Wasserstein kernel for persistence diagrams. In *Proceedings of the 34th International Conference on Machine Learning*, volume 70 of *Proceedings of Machine Learning Research*, pages 664–673, 2017.
- Chih-Chung Chang and Chih-Jen Lin. Libsvm: a library for support vector machines. *ACM transactions on intelligent systems and technology (TIST)*, 2(3):27, 2011.
- Frederic Chazal, Brittany Fasy, Fabrizio Lecci, Bertrand Michel, Alessandro Rinaldo, and Larry Wasserman. Subsampling methods for persistent homology. In *International Conference on Machine Learning*, pages 2143–2151, 2015.
- Chao Chen and Novi Quadrianto. Clustering high dimensional categorical data via topographical features. In *International Conference on Machine Learning*, pages 2732–2740, 2016.
- David Cohen-Steiner, Herbert Edelsbrunner, and John Harer. Stability of persistence diagrams. *Discrete & Computational Geometry*, 37(1):103–120, 2007.
- Vin De Silva, Robert Ghrist, et al. Coverage in sensor networks via persistent homology. *Algebraic & Geometric Topology*, 7(1):339–358, 2007.
- Barbara Di Fabio and Massimo Ferri. Comparing persistence diagrams through complex vectors. In *International Conference on Image Analysis and Processing*, pages 294–305. Springer, 2015.
- Herbert Edelsbrunner and John Harer. Persistent homology—a survey. *Contemporary mathematics*, 453:257–282, 2008.
- Herbert Edelsbrunner, David Letscher, and Afra Zomorodian. Topological persistence and simplification. In *Proceedings 41st Annual Symposium on Foundations of Computer Science*, pages 454–463, 2000.
- Stephen Richard Elliott. Physics of amorphous materials. *Longman Group, Longman House, Burnt Mill, Harlow, Essex CM 20 2 JE, England, 1983.*, 1983.
- Aasa Feragen, Francois Lauze, and Soren Hauberg. Geodesic exponential kernels: When curvature and linearity conflict. In *Proceedings of the IEEE Conference on Computer Vision and Pattern Recognition*, pages 3032–3042, 2015.
- Nicolas Francois, Mohammad Saadatfar, R Cruikshank, and A Sheppard. Geometrical frustration in amorphous and partially crystallized packings of spheres. *Physical review letters*, 111(14):148001, 2013.
- Leslie Greengard and John Strain. The fast gauss transform. *SIAM Journal on Scientific and Statistical Computing*, 12(1):79–94, 1991.
- Ying Guo, Peter L Bartlett, John Shawe-Taylor, and Robert C Williamson. Covering numbers for support vector machines. In *Proceedings of the twelfth annual conference on Computational learning theory*, pages 267–277, 1999.
- Zaid Harchaoui, Eric Moulines, and Francis R Bach. Kernel change-point analysis. In *Advances in neural information processing systems*, pages 609–616, 2009.
- Allen Hatcher. *Algebraic topology*. Cambridge University Press, 2002.

- Jan-Martin Hertzsch, Rob Sturman, and Stephen Wiggins. Dna microarrays: design principles for maximizing ergodic, chaotic mixing. *Small*, 3(2):202–218, 2007.
- Christoph Hofer, Roland Kwitt, Marc Niethammer, and Andreas Uhl. Deep learning with topological signatures. In *Advances in Neural Information Processing Systems*, pages 1633–1643, 2017.
- Jacques Istas. Manifold indexed fractional fields? *ESAIM: Probability and Statistics*, 16:222–276, 2012.
- Sadeep Jayasumana, Richard Hartley, Mathieu Salzmann, Hongdong Li, and Mehrtash Harandi. Kernel methods on riemannian manifolds with gaussian rbf kernels. *IEEE transactions on pattern analysis and machine intelligence*, 37(12):2464–2477, 2015.
- Peter M Kasson, Afra Zomorodian, Sanghyun Park, Nina Singhal, Leonidas J Guibas, and Vijay S Pande. Persistent voids: a new structural metric for membrane fusion. *Bioinformatics*, 23(14):1753–1759, 2007.
- Genki Kusano, Yasuaki Hiraoka, and Kenji Fukumizu. Persistence weighted gaussian kernel for topological data analysis. In *International Conference on Machine Learning*, pages 2004–2013, 2016.
- Genki Kusano, Kenji Fukumizu, and Yasuaki Hiraoka. Kernel method for persistence diagrams via kernel embedding and weight factor. *Journal of Machine Learning Research*, 18(189):1–41, 2018.
- Roland Kwitt, Stefan Huber, Marc Niethammer, Weili Lin, and Ulrich Bauer. Statistical topological data analysis—a kernel perspective. In *Advances in neural information processing systems*, pages 3070–3078, 2015.
- John Lafferty and Guy Lebanon. Diffusion kernels on statistical manifolds. *Journal of Machine Learning Research*, 6(Jan):129–163, 2005.
- Longin Jan Latecki, Rolf Lakamper, and T Eckhardt. Shape descriptors for non-rigid shapes with a single closed contour. In *Proceedings of the IEEE Conference on Computer Vision and Pattern Recognition (CVPR)*, volume 1, pages 424–429, 2000.
- Tam Le and Marco Cuturi. Adaptive euclidean maps for histograms: generalized aitchison embeddings. *Machine Learning*, 99(2):169–187, 2015a.
- Tam Le and Marco Cuturi. Unsupervised riemannian metric learning for histograms using aitchison transformations. In *International Conference on Machine Learning*, pages 2002–2011, 2015b.
- Hyekyoung Lee, Moo K Chung, Hyejin Kang, Bung-Nyun Kim, and Dong Soo Lee. Discriminative persistent homology of brain networks. In *International Symposium on Biomedical Imaging: From Nano to Macro*, pages 841–844, 2011.
- John M Lee. *Riemannian manifolds: an introduction to curvature*, volume 176. Springer Science & Business Media, 2006.
- Paul Levy and Michel Loeve. *Processus stochastiques et mouvement brownien*. Gauthier-Villars Paris, 1965.
- Shahar Mendelson. On the performance of kernel classes. *Journal of Machine Learning Research*, 4 (Oct):759–771, 2003.
- Ha Quang Minh, Partha Niyogi, and Yuan Yao. Mercer’s theorem, feature maps, and smoothing. In *International Conference on Computational Learning Theory*, pages 154–168. Springer, 2006.
- Vlad I Morariu, Balaji V Srinivasan, Vikas C Raykar, Ramani Duraiswami, and Larry S Davis. Automatic online tuning for fast gaussian summation. In *Advances in neural information processing systems*, pages 1113–1120, 2009.
- Claus Muller. *Analysis of spherical symmetries in Euclidean spaces*, volume 129. Springer Science & Business Media, 2012.

- Takenobu Nakamura, Yasuaki Hiraoka, Akihiko Hirata, Emerson G Escolar, and Yasumasa Nishiura. Persistent homology and many-body atomic structure for medium-range order in the glass. *Nanotechnology*, 26(30):304001, 2015.
- Ofir Pele and Michael Werman. Fast and robust earth mover’s distances. In *International Conference on Computer Vision*, pages 460–467. IEEE, 2009.
- Giovanni Petri, Paul Expert, Federico Turkheimer, Robin Carhart-Harris, David Nutt, Peter J Hellyer, and Francesco Vaccarino. Homological scaffolds of brain functional networks. *Journal of The Royal Society Interface*, 11(101), 2014.
- Gabriel Peyre and Marco Cuturi. *Computational Optimal Transport*. 2017. URL <http://optimaltransport.github.io>.
- Ali Rahimi and Benjamin Recht. Random features for large-scale kernel machines. In *Advances in neural information processing systems*, pages 1177–1184, 2008.
- Jan Reininghaus, Stefan Huber, Ulrich Bauer, and Roland Kwitt. A stable multi-scale kernel for topological machine learning. In *Proceedings of the IEEE conference on computer vision and pattern recognition (CVPR)*, pages 4741–4748, 2015.
- I. J. Schoenberg. Positive definite functions on spheres. *Duke Mathematical Journal*, 9:96–108, 1942.
- Shai Shalev-Shwartz and Shai Ben-David. *Understanding machine learning: From theory to algorithms*. Cambridge university press, 2014.
- Gurjeet Singh, Facundo Memoli, Tigran Ishkhanov, Guillermo Sapiro, Gunnar Carlsson, and Dario L Ringach. Topological analysis of population activity in visual cortex. *Journal of vision*, 8(8): 11–11, 2008.
- Alex J Smola, Zoltan L Ovari, and Robert C Williamson. Regularization with dot-product kernels. In *Advances in neural information processing systems*, pages 308–314, 2001.
- Katharine Turner, Sayan Mukherjee, and Doug M Boyer. Persistent homology transform for modeling shapes and surfaces. *Information and Inference: A Journal of the IMA*, 3(4):310–344, 2014.
- Cédric Villani. *Topics in optimal transportation*. Number 58. American Mathematical Soc., 2003.
- Kelin Xia and Guo-Wei Wei. Persistent homology analysis of protein structure, flexibility, and folding. *International journal for numerical methods in biomedical engineering*, 30(8):814–844, 2014.